Flow-Induced Nematic String Phase in Semidilute Wormlike Micelle Solutions

Ignatius A. Kadoma* and Jan W. van Egmond†

Department of Chemical Engineering, University of Massachusetts at Amherst, Amherst, Massachusetts 01003

(Received 14 July 1997)

We present a combination of flow-induced phenomena in a semidilute solution of connected wormlike micelles. These phenomena include a local isotropic-to-nematic transition and a flow-induced string phase. The experimental techniques include small-angle light scattering and 3D flow birefringence and enable a differentiation between contributions of convection, stress, and diffusion to the structural evolution and relaxation. Our results are in qualitative agreement with the two-fluid model of Brochard and De Gennes and the Turner and Cates model of a flow-induced 1D gel phase. [S0031-9007(98)06299-1]

PACS numbers: 83.50.By

Wormlike micelles are flexible, locally cylindrical aggregates of amphiphilic molecules. In aqueous solutions, the average lengths of these micelles can approach several microns [1,2] with typical radii of $\sim 20-25$ Å and persistence lengths of ~ 150 Å. Accordingly, the static and dynamics properties of these solutions are qualitatively similar to those of conventional flexible polymers [3], and may be classed as dilute, semidilute, and concentrated solutions. However, unlike polymers, micellar chains undergo reversible scission and recombination on a time scale dependent on the amphiphile, concentration of counterions, and temperature. Furthermore, the addition of counterions tends to increase micelle length and flexibility by screening electrostatic repulsion between amphiphile head groups. Recently, the possible formation of multiconnected networks due to transient cross-links between entangled micelles with sufficient counterion concentration has attracted much interest [4–6]. In these networks, the connection points are transient and free to slide along the micelle backbone much like a 1D gas. Since the transient connection points replace entanglement points, the viscosity of these solutions is dramatically reduced [5,6]. Direct visualization of branched micelles in aqueous solutions of pure surfactants [7] and of surfactant mixtures [8,9] by transmission electron microscopy at a cryogenic temperature has also been reported. While such images demonstrate micelle shape and persistence length, they cannot reveal dynamic behavior: an aspect that is important when considering practical applications in areas such as flow modification [10] and biological membranes [11].

In addition to the effects of counterions, structural changes due to the application of external flow are also particularly rich. Shear-induced isotropic-nematic transitions have been reported in highly concentrated solutions of wormlike micelles [12,13]. More recently, Roux *et al.* [14] used rheology, rheo-optical techniques, and small angle neutron scattering (SANS) to investigate the orientation and texture properties of nematic solutions in shear flow. Kadoma and van Egmond [15] have reported shear-induced "phase separation" in semidilute solutions by small angle light scattering (SALS). The analogy between wormlike micellar and polymeric systems survives even for such exotic phenomena: Shear-induced phase separation has also been reported in semidilute polystyrene solutions in poor solvent [16], and results from a coupling between local fluctuations in concentration and stress. For similar semidilute, poor polymer solutions, Hashimoto and Kume [17] observed a novel flow-induced structure comprised of flow-aligned strings of relatively higher concentration than the bulk phase. Hamilton *et al.* [18] and Butler *et al.* [19] have looked at shear-induced hexagonal ordering and the kinetics of shear-induced alignment and decay in a highly entangled dilute micellar system using SANS. With this technique, they were able to probe individual micelles. In this report, however, we probe both clusters of micelles using SALS and individual micelles using 3D birefringence and relate a remarkable combination of flow-induced phenomena in a semidilute solution of connected wormlike micelles. These phenomena include a local isotropic-nematic transition in the individual micelles and a flow-induced mesoscopic string phase. Furthermore, we experimentally differentiate the contributions of convection, stress, and diffusion to structural evolution and relaxation. Also, in our recent paper [15], we show that the structural transitions have a hierarchy of effects that depend on salt concentration.

Polarized (V_V) and depolarized (H_V) SALS under shear were used to probe the mesoscopic structure of concentration and orientation fluctuations on inception of flow, at steady state, and during relaxation after flow cessation. Flow birefringence was used to measure average micelle orientation in 3D space. The system under investigation was a semidilute solution consisting of 0.03 M cetyltrimethylammonium bromide (CTAB) and an added counterion in the form of sodium salicylate (NaSal), prepared with a salt to amphiphile molar ratio of 8:1 in distilled water. The high salt concentration ensures the system is a multiconnected network [4–6,15,20,21]. All experiments were performed at room temperature using a linear parallel plate flow cell described in a previous study (see Fig. 2 of Ref. [20]), except that linear polarizers were placed on either side

of the flow cell for the SALS experiment. The optical train used for 3D flow birefringence is described in detail elsewhere [22].

By virtue of their elongated structure, wormlike micelles are optically anisotropic. Hence, scattered light can arise from both orientation fluctuations of the optically anisotropic scattering elements and/or concentration fluctuations. These contributions can be separated by comparisons of H_V with V_V scattering experiments because light scattered from concentration fluctuations will retain the polarization of the incident light. On the other hand, only orientation fluctuations result in depolarized H_V scattering.

H_V scattering was measured by setting the polarization of the incident beam at 45° to the flow direction and observing the scattered light through a polarized analyzer crossed with respect to the incident beam. V_V scattering was measured by setting the polarization of the incident beam and the analyzer along the flow direction. The geometry of the experiment dictated that scattering is obtained in the plane of flow and vorticity, i.e., q_x-q_z plane; where $\boldsymbol{q}$ is the scattering vector defined by $|\boldsymbol{q}| = (4\pi n/\lambda)\sin(\theta/2)$, θ is the scattering angle, n is the bulk refractive index of the medium, and λ is the wavelength of light in a vacuum. The time-dependent growth and relaxation of the V_V and H_V scattering patterns at a shear rate $\dot{\gamma} = 4\ \mathrm{s}^{-1}$ are shown in Fig. 1. The direction of flow (the q_x axis) is as indicated by the arrow, flow inception is at $t = 0$ s, and cessation is at $t = 25$ s. For no flow ($t = 0$ s), there is no scattering, indicating that the length scale of heterogeneities in the solution are much smaller than the wavelength of light. Shortly after flow inception [Fig. 1(c)] V_V scattering displays an intense fourfold pattern superimposed on a narrow bright streak at low q values along the vorticity direction. As steady state is reached, the fourfold pattern increases in intensity and merges into a twofold pattern [Fig. 1(e)]. On flow cessation, at $t = 25$ s, the intense streak rapidly disappears, and a butterfly pattern characterized by two high intensity lobes that extend to high q_x values appears [Fig. 1(i)]. The butterfly pattern then relaxes [Fig. 1(k)] and disappears as the system returns to its quiescent state. The H_V scattering follows a similar trend during flow: A fourfold pattern appears during start-up [Fig. 1(d)], followed by a twofold pattern along the vorticity direction during steady state [Fig. 1(f)]. It is, however, apparent that the high intensity streak at low q_z values is absent [Figs. 1(d) and 1(f)]. Also, on flow cessation, there is a remarkable difference in the relaxation of the scattering patterns: The fourfold H_V pattern [Figs. 1(h), 1(j), and 1(l)] decays monotonically and much more rapidly than the V_V pattern.

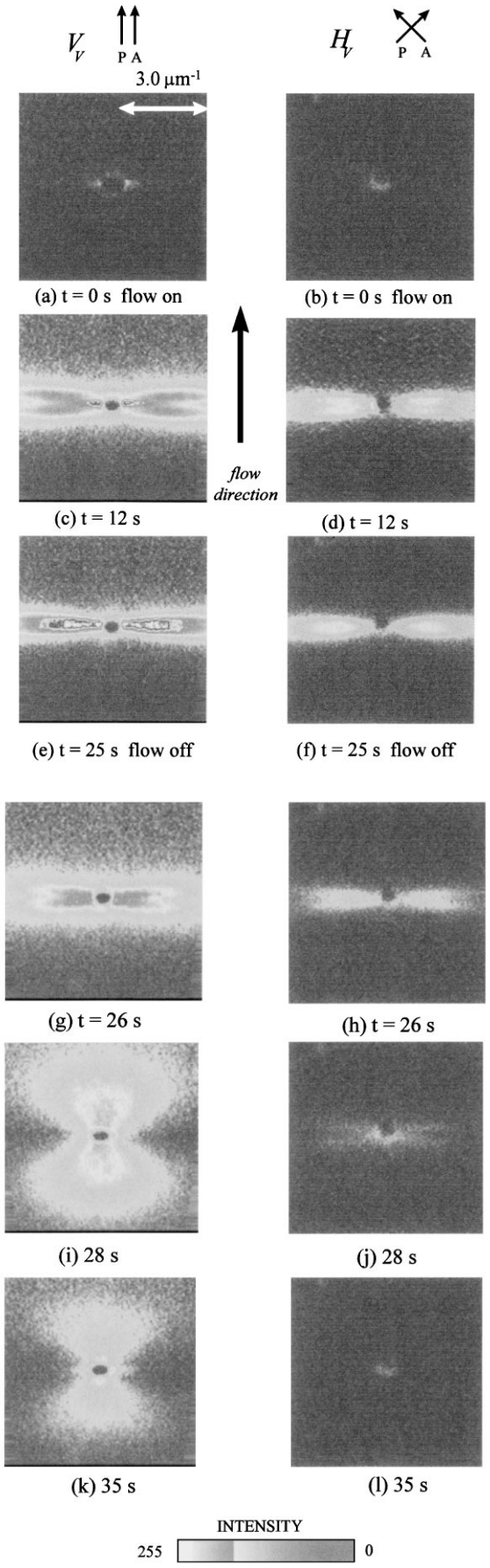

FIG. 1. Time-dependent V_V and H_V scattering patterns of a CTAB/NaSal solution with an amphiphile:salt ratio of 1:8 and shear rate $\dot{\gamma} = 4\ \mathrm{s}^{-1}$, temperature = 23 °C.

In order to understand the origin of the V_V scattering patterns, it is helpful to consider the physical processes that lead to shear-enhanced concentration fluctuations as predicted by two-fluid hydrodynamic models [23–26] that include a coupling term between the local polymeric or micellar viscoelastic stress and spatial inhomogeneity in concentration. The result of this coupling is the anisotropic enhancement of concentration fluctuations along the flow direction (q_x axis) and a suppression in the orthogonal direction. At small wave numbers q, the micelle stress characterized by a time scale $\tau_s = 2.9$ s follows rapidly the temporal variations in local concentration characterized by a time scale $1/Dq^2$, where D is the cooperative diffusion coefficient given by 13.6 $\mu m^2 s^{-1}$ [15]. However, at wave numbers larger than a characteristic wave vector q^*, defined by $D(q^*)^2 = 1/\tau_r$, the flow enhancement mechanism breaks down because concentration fluctuations relax faster than stress. Hence, scattering decreases for $q > q^*$ [26], resulting in a scattering peak located at q^*. In addition, convection affinely deforms concentration fluctuations and at sufficiently high shear rates results in elongated regions of high concentration stretched along the flow axis. The competition of these mechanisms, in addition to diffusive osmotic forces, determines the evolution and relaxation of concentration fluctuations that can be probed by V_V scattering experiments.

At low shear rates or salt concentration, the stress-enhancement mechanism dominates, but the results in that regime have been reported elsewhere [15]. At the relatively high shear rate presented in this report, convection dominates the stress-enhancement mechanism deforming concentration fluctuations along the directions of average micelle orientation. The result is a so-called string phase [Figs. 2(a) and 2(b)] characterized by generally flow-aligned strings of relatively high micelle concentration compared to the low concentration bulk phase [17] and is observed by the bright V_V streak at low q_z values [Fig. 1(c)]. The appearance of H_V patterns [Figs. 1(d) and 1(f)] implies that the strings are nematic. Initially, the strings themselves form a connected network stretched along the flow direction [Fig. 2(a)]. The fourfold H_V pattern, with scattering at high q values and squashed towards the vorticity direction [Fig. 1(d)], corresponds to correlations between orientation fluctuations within the network of strings [Fig. 2(a)]. As the system approaches steady state, the string network relaxes by flow aligning, and the fourfold pattern merges into a twofold H_V pattern normal to the flow direction. A mechanism by which this relaxation can occur is by the increased probability of reactions combining micelles end-to-end due to the increased micellar orientation within the strings. The result is the formation of a population of flow-aligned, giant micelles. Indeed, the flow-induced appearance of giant micelles (or 1D gel) has recently been predicted by Turner and Cates [27]. The twofold H_V pattern thus corresponds to orientational correlations of elongated, highly flow-aligned individual strings [Fig. 2(b)].

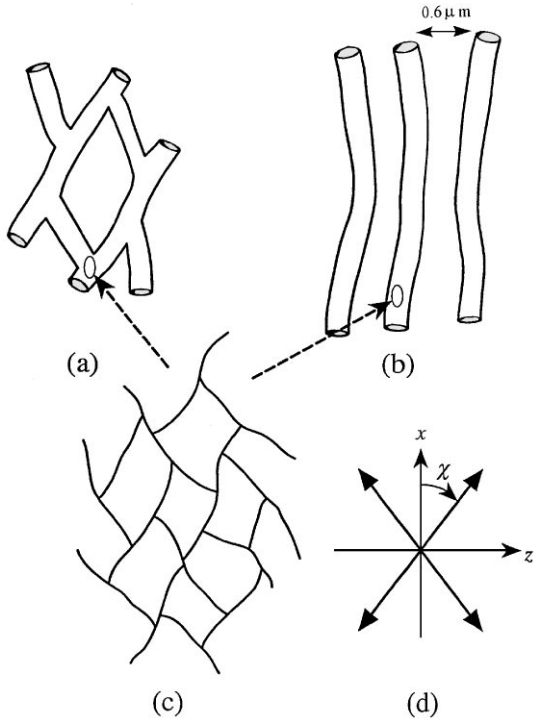

FIG. 2. Schematic of multiconnected network showing proposed response to a uniform flow field (a) flow-aligned network of strings; (b) giant strings oriented in flow direction; (c) degenerate nematic network in frustrated state at finite angle χ to the flow direction (d).

Within the strings, however, micelles appear to retain a considerable degree of their connected structure. This is confirmed by the results of 3D flow birefringence which probes average micelle orientation. The anisotropy of the refractive index tensor in the x-z plane, $N_3 \equiv n_{xx} - n_{zz}$ is approximately 2 orders of magnitude less than the anisotropy in the x-y plane $N_1 \equiv n_{xx} - n_{yy}$ (Fig. 3). Since optical anisotropy is directly proportional to micelle orientational anisotropy, $N_3 \ll N_1$ implies that micelles have significant orientation along both the flow and vorticity directions relative to the velocity gradient direction (y axis). This structure is possible because, within the strings, the higher concentration causes connection points to come closer together. However, as long as the network remains intact, the finite flexibility of the micelles and the reduced distance between connection points dictate that micelles cannot orient perfectly along the flow direction. Instead, a frustrated state emerges where micelle orientation must be at a finite angle χ to the flow direction [Figs. 2(c) and 2(d)]. This frustrated state can also be thought of as a nematic phase with two degenerate director orientation angles $\pm\chi$, and with micelles free to translate along their backbone because of the transient connection points.

The sequence of relaxation behavior on flow cessation can be explained as follows. First, the nematic strings

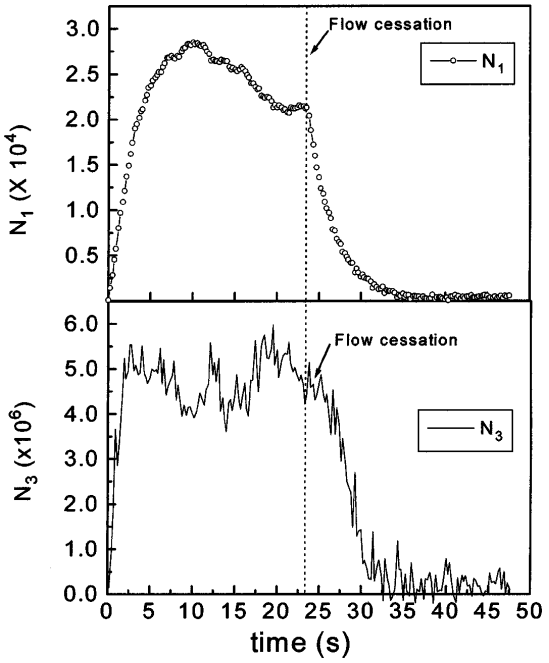

FIG. 3. Time-dependent behavior of optical anisotropy $N_1 \equiv n_{xx} - n_{yy}$ and $N_3 \equiv n_{xx} - n_{zz}$ for a 1:8 CTAB/NaSal solution at shear rate $\dot{\gamma} = 4\ s^{-1}$, temperature = 23 °C. Start-up of flow at $t = 0$ s and flow cessation at $t = 23$ s.

rapidly break up into droplets of relatively high concentrated micelles. After approximately three seconds, due to residual micellar stresses in the system, the concentration fluctuations corresponding to the droplets are enhanced along the flow direction by the stress-concentration coupling mechanism. This results in the butterfly pattern oriented along the flow direction [Fig. 1(i)] that is typical of this type of mechanism [15,16]. Thereafter, as the residual stresses relax, the butterfly pattern relaxes through a coupling between diffusion and stress [16,26]. Under crossed polarizers, only orientational fluctuations during the breakup of the nematic string structure contribute to scattering. The sequence here is the reverse of the flow alignment procedure as the system relaxes from flow-aligned, nematic strings to a degenerate nematic [Fig. 1(j)] and finally to an isotropic multiconnected network [Fig. 1(k)].

The financial support of 3M Corporation and the National Science Foundation under Grant No. DMR 94-00488 (MRSEC) is greatly appreciated.

*Current address: Specialty Adhesives and Chemicals Division, 3M Center, 236-3D-01, St. Paul, MN 55144-1000.

†To whom correspondence should be addressed.

[1] V. Degiorgio and M. Corti, in *Physics of Amphiphiles: Micelles, Vesicles and Microemulsions* (Elsevier, New York, 1985).

[2] M. E. Cates and S. F. Candau, J. Phys. Condens. Matter **2**, 6869 (1990).

[3] S. J. Candau, E. Hirsch, and R. Zana, in *Physics of Complex Supermolecular Fluids* (Wiley, New York, 1987), pp. 569–584.

[4] J. Appell, G. Porte, A. Khatory, F. Kern, and S. J. Candau, J. Phys. II (France) **2**, 1045 (1992).

[5] G. Porte, R. Gomati, O. El Haitami, J. Appell, and J. Marignan, J. Phys. Chem. **90**, 746 (1986).

[6] A. Khatory, F. Kern, F. Lequeux, J. Appell, G. Porte, N. Morie, A. Ott, and W. Urbach, Langmuir **9**, 933 (1993).

[7] D. Danino, Y. Talmon, H. Levy, G. Beinert, and R. Zana, Science **269**, 1420 (1995).

[8] P. K. Vinson, J. R. Bellare, H. T. Davis, W. G. Miller, and E. Scriven, J. Colloid Interface Sci. **142**, 74 (1991).

[9] P. K. Vinson and Y. Talmon, J. Colloid Interface Sci. **133**, 288 (1989); L. Magid, J. Gee, and Y. Talmon, Langmuir **6**, 1609 (1990).

[10] H. Rehage and H. Hoffmann, J. Phys. Chem. **92**, 4712 (1988); H. Rehage and H. Hoffmann, Mol. Phys. **74**, 933 (1991).

[11] C. A. Lawrence, in *Cationic Surfactants*, edited by E. Jungermann (Marcel Dekker, New York, 1970), p. 491.

[12] J. F. Berret, D. C. Roux, G. Porte, and P. Lindner, Europhys. Lett. **25**, 521 (1994).

[13] V. Schmitt, F. Lequeux, A. Pousse, and D. Roux, Langmuir **10**, 955 (1994).

[14] D. C. Roux, J.-F. Berret, G. Porte, E. Peuvrel-Disdier, and P. Lindner, Macromolecules **28**, 681 (1995).

[15] I. A. Kadoma and J. W. van Egmond, Langmuir **13**, 4551 (1997).

[16] X.-L. Wu, D. J. Pine, and P. K. Dixon, Phys. Rev. Lett. **66**, 2408 (1991); J. W. van Egmond, D. E. Werner, and G. G. Fuller, J. Chem. Phys. **96**, 7742 (1992).

[17] T. Kume and T. Hashimoto, in *Flow Induced Structure in Polymers* (American Chemical Society, Washington, DC, 1995), Vol. 597, pp. 35–47.

[18] W. A. Hamilton, P. D. Butler, S. M. Baker, G. S. Smith, J. B. Hayter, L. J. Magid, and R. Pynn, Phys. Rev. Lett. **72**, 2219 (1994).

[19] P. D. Butler, L. J. Magid, W. A. Hamilton, J. B. Hayter, B. Hammouda, and P. J. Kreke, J. Phys. Chem. **100**, 442 (1996).

[20] I. A. Kadoma, C. M. Ylitalo, and J. W. van Egmond, Rheol. Acta **36**, 1 (1997).

[21] I. A. Kadoma and J. W. van Egmond, Phys. Rev. Lett. **76**, 4432 (1996).

[22] S. Kalogrianitis and J. W. van Egmond, J. Rheol. **41**, 343 (1997).

[23] F. Brochard and P. G. de Gennes, Macromolecules **10**, 1157 (1977).

[24] E. Helfand and G. H. Fredrickson, Phys. Rev. Lett. **62**, 2468 (1989).

[25] M. Doi and A. Onuki, J. Phys. II (France) **2**, 1631 (1992).

[26] S. Milner, Phys. Rev. E **48**, 3674 (1993).

[27] M. S. Turner and M. E. Cates, J. Phys. Condens. Matter **4**, 3719 (1992).